

**FINAL REPORT TO THE  
U.S. ARMY WHITE SANDS MISSILE RANGE  
UNDER CONTRACT NO. ASL89-8016**

**("Field Test of a New Lidar System at White Sands")**

**Prepared for U. S. Army**

**by**

**Lawrence F. Radke, Charles A. Brock and Peter V. Hobbs  
Cloud and Aerosol Research Group  
Atmospheric Sciences Department  
University of Washington  
Seattle, WA 98195  
USA**

**The statements and conclusions in this report are those of the contractor and not necessarily those of the U. S. Army. The mention of commercial products, their source or their use in connection with material reported therein is not to be construed as either an actual or implied endorsement of such products.**

**June 16, 1989**

## TABLE OF CONTENTS

	<u>Page</u>
1. INTRODUCTION	1
1.1 <i>The planetary boundary layer</i>	1
1.2 <i>Cirrus clouds</i>	2
1.3 <i>Atmospheric extinction</i>	2
2. THE UNIVERSITY OF WASHINGTON-GEORGIA TECH LIDAR SYSTEM	3
3. DATA ANALYSIS	6
4. RESULTS	8
4.1 <i>Operational difficulties</i>	8
4.2 <i>Lidar-derived profiles</i>	9
5. RECOMMENDATIONS FOR FUTURE WORK	23
6. CONCLUSIONS	25
7. REFERENCES	25

# FIELD TEST OF A NEW LIDAR SYSTEM AT WHITE SANDS

## 1. INTRODUCTION

This report describes the initial testing and field use of a monostatic, ground-based, upward-pointing lidar at the U. S. Army White Sands Missile Range (WSMR) in February 1989. The purpose of the project was to test the ability of the lidar to provide information on the structure of the planetary boundary layer (PBL), to detect visible and subvisible cirrus clouds, and to derive profiles of atmospheric optical extinction for comparison with *in situ* aircraft measurements made nearby.

Lidar has been used extensively since the late 1960s to probe the optical properties of the atmosphere remotely (for a review of the early use of lidar, see Collis and Russell, 1976). The principle of the lidar is similar to that of conventional radar: an outgoing beam of electromagnetic radiation is scattered by targets, and the return signal is detected. In the case of meteorological radars, the target is generally precipitation; with lidars, smaller aerosol particles and gas molecules are often the targets.

The development of inexpensive, stable, relatively high-energy lasers in recent years has spurred the use of lidars in atmospheric remote sensing. Three areas of lidar applications--detecting the PBL, sensing cirrus clouds, and estimating vertical profiles of atmospheric optical extinction--are of particular relevance to operations at WSMR. A brief review of each of these topics follows.

### 1.1 *The planetary boundary layer*

The PBL is the region of the lower troposphere the properties of which are directly controlled by interactions with the surface. The PBL is often turbulent; this mixing results in approximate vertical homogeneity for a number of parameters (e.g., temperature, humidity, particle concentrations). Because there is often a sharp gradient in aerosol particle properties and concentrations between the PBL and the overlying free troposphere, lidar can be used to detect the height of the PBL. Lidars have

also proven to be a useful for studying the structure and development of the PBL (e.g., Martin *et al.*, 1988; Melfi *et al.*, 1985; McElroy *et al.*, 1981).

Lidar has been shown to be most effective in studying the PBL when used in one of the following ways. 1) Pointing downward from an airborne platform. 2) Scanning from horizon to zenith (in a range-height indicator mode). 3) Pointing upward from the surface in a fixed position. When used in the fixed, upward-pointing mode, the laser beam must diverge rapidly enough to fill a significant portion of the telescope's field of view before the beam has passed through the PBL. Thus, lidar systems designed for fixed, upward-pointing observations of the PBL typically have large laser beam divergences (4 mrad or more). A disadvantage of such lidars is that they lose sensitivity at distances of more than a few kilometers.

## 1.2 *Cirrus clouds*

Cirrus clouds occur with surprisingly high frequency over large regions of the globe (e.g., Warren *et al.*, 1986; Wylie and Menzel, 1989). Such clouds are important for a variety of reasons, including stratospheric chemistry (Salawitch *et al.*, 1988), radiative transfer (Platt, 1973; SMIC, 1971; Reed, 1982), and aeronautical operations and weapons applications (Waggoner and Radke, 1989). Some cirrus clouds (termed "subvisible cirrus") do not display haloes, sun dogs and parhelia, and are difficult to detect. Lidar is one of few methods for detecting subvisible cirrus (Sassen *et al.*, 1989), mapping its vertical and temporal variations, and providing information on the radiative properties of these clouds (e.g., Platt, 1979).

## 1.3 *Atmospheric extinction*

Lidar has been shown to be very useful in deriving profiles of atmospheric optical extinction, which are used in calculations of radiative transfer through the atmosphere (e.g., Wendling *et al.*, 1985). The effect of aerosol particles on the earth-atmosphere radiative balance is described by the

vertical distribution of the extinction and absorption properties of the aerosol. Visibility, or meteorological range, may be estimated from extinction coefficient using the relation developed by Koschmieder (1924):  $V_r = \frac{3.91}{\sigma_e}$ , where  $V_r$  is the meteorological range and  $\sigma_e$  the extinction coefficient.

While most lidars do not measure extinction directly (a notable exception is high spectral resolution lidar, HSRL, described by Shipley *et al.*, 1983 and Sroga *et al.*, 1983), relationships between backscatter coefficients and extinction coefficients may be used to derive the extinction profile (e.g., Kunz, 1983). These relationships are based either on in situ measurements of the optical properties of the aerosol being observed (e.g., Salemink *et al.*, 1984), or on relationships calculated from Mie theory using measured or assumed particle size distributions, morphology and composition (van de Ven *et al.*, 1980). Another method for deriving a relationship between extinction and backscatter and for calibrating a ground-based lidar is to make multiple profiles of backscatter within the PBL at various angles. The so-called "slope method" can then be used to calibrate the system and extract the desired relationship (e.g., Spinhirne *et al.*, 1980; Klett, 1981; Eloranta and Forest, 1986).

## 2. THE UNIVERSITY OF WASHINGTON-GEORGIA TECH LIDAR SYSTEM

The lidar used at WSMR was designed and built at Georgia Tech Research Institute (GTRI) in Atlanta, Georgia, under contract with, and to meet specifications set forth by, the University of Washington (UW). This lidar was constructed largely with "off-the-shelf" components that have become available in recent years. The lidar is to be incorporated into the UW's Convair C-131A research aircraft.

Figure 1 shows a schematic diagram of the lidar system and Table 1 gives system specifications. Polarized, incoherent, monochromatic light is emitted from the neodymium-doped yttrium aluminum garnet (Nd:YAG) laser simultaneously at both the primary (1.064  $\mu\text{m}$ ) and frequency-doubled (0.532  $\mu\text{m}$ ) wavelengths. The beam is reflected by a mirror  $90^\circ$  toward the center line of the telescope assembly. The beam is then reflected by another mirror and is emitted upward along the axis of the

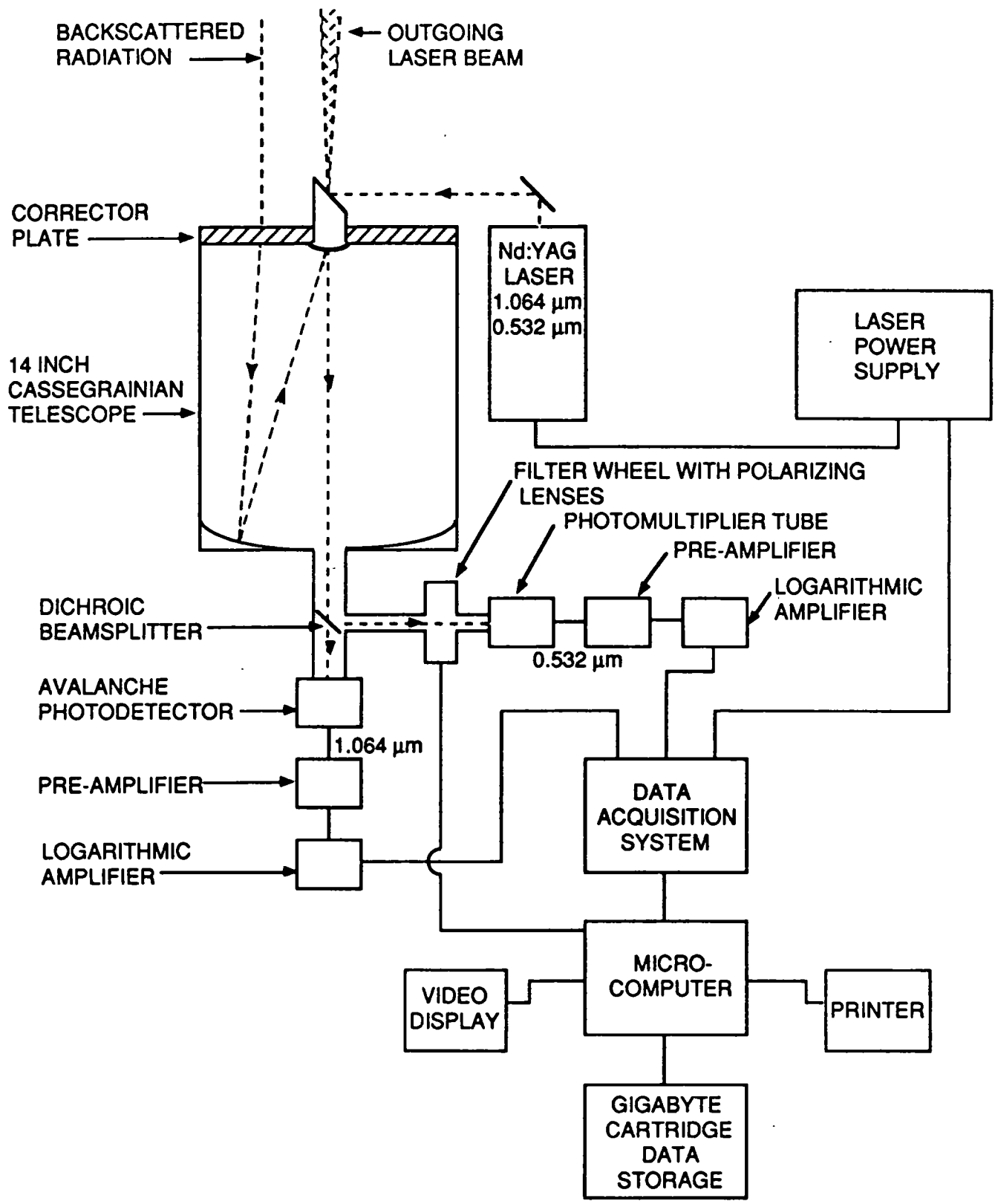


Figure 1. Schematic of the University of Washington-Georgia Tech Lidar System

Table 1. Specifications for the University of Washington-Georgia Tech lidar system

---

A) Laser

Type: Neodymium-doped Yttrium Aluminum Garnet  
Wavelengths: 1.064 and 0.532  $\mu\text{m}$   
Energies: 70 and 45 mJ  
Pulse width: 20 ns  
Beam divergence: 1 mrad

B) Telescope

Type: Cassegrainian  
Diameter: 0.356 m (14 in)

C) Detection

Polarizing filters: selectable for parallel and perpendicular polarizations  
Detectors: 1.064  $\mu\text{m}$   
Type: Silicon Avalanche Photodiode  
0.532  $\mu\text{m}$   
Type: Photomultiplier tube

D) Data acquisition/control system

Data input and shot summing  
Type: CAMAC crate  
Manufacturer: DSP Technologies, Inc.  
Digitization rate: 25 ns or 50 ns

Control/display computer: IBM PC model AT  
Data display: EGA monitor, dot-matrix printer  
Data storage: 20 megabyte hard disk, floppy disks, or  
1.2 gigabyte mini-video cassettes

---

telescope. Alignment of the laser beam with the telescope is controlled by adjusting the second mirror. The emitted laser pulse, which has a pulse width of 20 ns (or 6 m) and energies of 70 mJ at 1.064  $\mu\text{m}$  and 45 mJ at 0.532  $\mu\text{m}$ , travels upward while diverging at an angle of approximately 1 mrad. The laser pulse interacts with gas molecules, aerosol and cloud particles, returning a small fraction of the energy as backscattered light at the same wavelengths. This return pulse is received and focused by the 0.356 m (14 in.) Cassegrainian telescope.

After the light passes through the telescope, it strikes a dichroic mirror. This beamsplitting device allows the infrared wavelength to pass without reflection; the visible light is reflected  $90^\circ$ . The 1.064  $\mu\text{m}$  beam is detected by a silicon avalanche photodiode (APD), while the visible light is sensed with a photomultiplier tube (PMT). The signals from each of these detectors pass through separate pre-amplifiers (to convert current to voltage) and logarithmic amplifiers. The logarithmic amplifiers are needed to detect a wide range of signal strengths without electronic saturation.

The amplifier outputs are received by a data acquisition system (DAS, DSP Technologies, Inc.), which has a variable signal digitization rate of 25 or 50 ns, corresponding to vertical resolutions of 7.5 and 15 m, respectively. The data are summed in the DAS for a user-specified number of laser shots, and are then dumped to an IBM AT microcomputer through an input board supplied with the DAS. A menu-driven program on the microcomputer is used to record the data on a 20 mb hard disk and to display individual shot profiles. The shot records are then dumped to floppy disks for permanent storage. (Since the test at WSMR, the data system has been reconfigured to store the data on 1.2 gigabyte mini-video cassettes. Also, software has been developed to display real-time, two-dimensional time/height color cross-sections.)

### 3. DATA ANALYSIS

The signal received by the detectors on the lidar is described through the lidar equation:

$$P(r) = \frac{C[B_p(r) + B_g(r)]}{r^2} \exp\left(-2 \int_0^r \sigma_e(r) dr\right) + M \quad (1)$$

where  $P(r)$  is the power of the returned signal,  $C$  a system constant that depends upon telescope parameters and the output power of the laser,  $\beta_p$  and  $\beta_g$  are the volume backscatter coefficients due to particles and gas molecules, respectively,  $r$  the distance from the lidar to the target,  $\sigma_e$  the extinction coefficient due to both aerosols and gas molecules, and  $M$  the contribution from multiple scattering. The exponential term accounts for loss of laser power due to extinction of the laser pulse as it travels from the lidar to the target and back. Note that the backscatter and extinction coefficients are functions of wavelength; a separate solution is required for each laser wavelength.

To solve the lidar equation, a relation must be found between backscatter and extinction (e.g. Klett, 1981), or the exponential (extinction) term may be ignored (e.g. Wendling *et al.*, 1985). In turbid atmospheres, the extinction term must be retained in the solution. For clear atmospheres, the contribution of this term is negligible, as is that for the multiple scattering term. If the extinction term is retained, a boundary value must be specified at some point in the lidar profile, or an iterative solution may be used. In the test study at WSMR, visibilities were quite high below mid-level clouds. Therefore, we have chosen to neglect the exponential terms and multiple scattering in the lidar equation.

The lidar signal must be corrected for the range-squared dependence of the laser power, and for the logarithmic response of the signal amplifiers. The response of the amplifiers (the digital counts per decibel of signal) must be known. As we will discuss later, various problems with the amplifiers (discovered during post analysis of the field data) precluded quantitatively accurate extraction of the lidar power for much of the project at WSMR. As a result, we do not have great confidence in the extinction profiles that we have derived.

It should be noted that this was the first field use of the UW/GT lidar, and that some components, most notably the APD, were not installed until two weeks before the project at WSMR. Further work on the lidar should quickly remove the uncertainties associated with the logarithmic amplifiers, allowing for more complete, quantitative evaluation of the lidar signals from future projects.

## 4. RESULTS

### 4.1 *Operational difficulties*

A number of operational difficulties were encountered during the project at WSMR . The first of these was caused by the location of the experiment in an active military weapons testing and flight operations area. Due to concerns about the safety of military aircraft maneuvers near the lidar site, atmospheric testing of the lidar was severely restricted. Permission to use the lidar was granted verbally by the Range Control Officer. However, blocks of time that were initially allocated for operation of the lidar were subsequently often fragmented by military operations of higher priority. As a result, there was often little time to set up the lidar, test it, correct obvious problems, and begin collection of reliable data.

The brevity of the time blocks that the lidar operated in would have been relatively inconsequential if the lidar had performed perfectly. However, a number of electrical problems were encountered. Some of these were correctable in the field, but others were not. The bulk of the difficulties could be traced to the necessity of repeatedly installing and moving the lidar, and to electronic problems in the logarithmic amplifiers. The lidar system was mounted on the back of a flatbed truck that was backed up to an enclosed trailer. The telescope, laser assembly, detectors and amplifiers were located on a rigid rack on the truck. Shielded cables 3-5 m long were required to connect the optical assembly to the power supplies, data system and computer within the trailer. The optical assembly was moved into the trailer after operation of the lidar to protect the sensitive components. The trailer was partially warmed by a small space heater; the optical assembly was unprotected.

Despite the electronic shielding of the cables connecting the telescope assembly and the data system, signals induced by the power supplies for the lidar and amplifiers for the detectors, as well as interference from unknown sources, were sometimes superimposed on the lidar return. These spurious signals were most often apparent in the near-field (low-altitude) return signal. As a result, boundary layer features were sometimes obscured. Other signals could be seen near the end of the lidar return at

12-15 km altitude. These induced signals ("noise") were relatively weak and did not obscure cloud signatures.

Moving the lidar from the trailer to the flatbed truck also produced electrical problems. Electrical connections that were secure in the laboratory became loose during the movement, causing noise in the return signal. Troubleshooting the entire system--a time consuming task--became necessary at the start of each operational period. Because of the short length of the allocated time blocks for operation, considerable quantities of potentially useful data were lost.

A final difficulty encountered during the project was the erratic behavior of two of the amplifiers. The signal from the infrared amplifier did not display the expected logarithmic response. As discussed below, this problem has been traced to incomplete installation instructions from the manufacturer. Also, the gain on the amplifier operating on the visible wavelength fluctuated without warning. This problem is believed to be due to a faulty transistor in the amplifier that may have been badly jarred during shipping. A cracked corrector plate on the well-protected telescope attests to the extremely rough handling that the lidar received while being shipped to WSMR.

#### *4.2 Lidar-derived profiles*

Despite the difficulties described above, the lidar showed excellent sensitivity. Thin cirrus clouds were detected at both wavelengths. Cirrus clouds were observed at altitudes as great as 12 km above a layer of altocumulus during both daytime and nighttime hours. This sensitivity was due to the relatively high power of the laser, the slow divergence of the emitted pulse, and good optical sensitivity of the telescope. There was no apparent effect on the performance of the telescope due to the damaged corrector plate.

Results are presented in two forms: time-height cross-sections of the lidar return signal, and vertical profiles of the lidar return signal and derived extinction values. Table 2 lists the times and

Table 2. Lidar operating periods in which valid data were taken

(a) 8 February 1989

Times (local)*	Pulse rate (hz)	Shots per record	Comments†
0820-0853	1	55	Strong return from As/Ac ~4.2 km.
0853-0914	1	55	Strong return from As/Ac ~4.8 km.
0953-1058	1	55	Thin Ac and Ci from 5.5-7.5 km.
1422-1434	10	100	Thick Ac. Ci above to 9km.
1437-1443	10	100	Weak returns from Ci ~6.5 km.
1456-1458	10	10	Strong Ac/As ~4.8 km. No Ci seen
1501-1524	2	100	Strong Ac/As ~4.8 km. No Ci seen
1525-1530	2	100	Strong Ac/As ~4.8 km. No Ci seen
1926-1947	10	100	Multiple As/Ac from 4-7.5km. PBL apparent
1950-2006	10	100	Multiple As/Ac from 4-7.5km. Very thin Ci at 8.5 km.
2007-2023	10	100	PBL visible. Ci at +10 km. .
2024-2039	10	100	Much Ci to 11km; some lower at 6 km.
2040-2057	10	100	Much Ci to 11km; some lower at 6 km.
2057-2100	10	100	Much Ci to 11km; some lower at 6 km.

(b) 9 February 1989

Times (local)*	Pulse rate (hz)	Shots per record	Comments†
1001-1034	5	55	Strong PBL structure. Liquid clouds at 4.5km. Ci at 9 km.
1039-1047	10	100	Some ice cloud at 4 km. Ci at +8.5 km.
1132-1140	10	55	Very strong PBL signal. Some cloud at 4 km.
1141-1159	10	100	Very strong PBL signal. Ci at 9.5 km.
1200-1216	10	100	Very strong PBL signal. No cloud.
1405-1442	5	100	PBL strong Ci at 9 km from contrails (liquid?)
1442-1509	5	100	PBL light. Ci at 9.5 km--contrail blow-off.
1521-1545	5	100	PBL very weak. Ci at 9.5 km.
1545-1559	5	100	No Ci.

\* The indicated times bracket individual computer files composed of records containing averages of the return pulses from laser firings. The last entry, for example, contains 15 minutes of 20-second average profiles from the lidar, which was being fired at 5 pulses per second.

† AC=altocumulus; As-altostratus; Ci-cirrus; PBL-planetary boundary layer..

mode of operation of the lidar during the test at WSMR. Data were collected for a total of 6.7 hours during two days of lidar operations.

The infrared (1.064  $\mu\text{m}$ ) wavelength results proved superior to the visible (0.532  $\mu\text{m}$ ) data for visualization of atmospheric structure. This can be attributed to two factors: the reduction by a factor of 16 in gas molecule (Rayleigh) backscattering in the infrared compared to the visible, and the better stability of the logarithmic amplifier at this wavelength.

Although the amplifier was more stable at 1.064  $\mu\text{m}$  than at 0.532  $\mu\text{m}$ , numerous problems were encountered in attempting to extract quantitative backscatter information from the lidar return at 1.064 $\mu\text{m}$ . These problems have been traced to incorrect instructions from the manufacturer on the installation of the amplifier unit (an improper resistor was used). The electrical configuration of the amplifier has recently been corrected; however, there is no known way to correct the data taken at WSMR *ex post facto*.

Figure 2A shows a range- and logarithm-corrected profile of 100 averaged infrared lidar shots taken near 1930 MST on 8 February 1989 (line "a"). There is an obvious problem with the signal in the first 1.2 km of the profile--the signal drops very rapidly and then becomes virtually flat until the clouds are detected at  $\sim$ 4.2 km. This dropoff is not due to enhanced scattering in the PBL; it is an artifact introduced by the faulty amplifier. We do believe, however, that the "bulge" in the return signal at about 1 km is due to aerosol scattering near the top of the boundary layer. This same feature was observed on the visible wavelength return and was persistent, unlike other transient noises superimposed on the signal. There is no apparent drop in signal above 1 km that could be attributed to Rayleigh scattering, which should decrease logarithmically with height. The Rayleigh backscatter signal (as calculated from a climatological average sounding for February at nearby El Paso, Texas, and normalized to the lidar return at 3.5 km) is given by the line marked "b" in Fig. 2A. To enhance the boundary layer signal, a third order polynomial was fitted to the return signal below 1.2 km and subtracted from the signal below this level. This polynomial is the line marked "c" in Fig. 2A. While this is an arbitrary technique to "correct" the data for the electronic problems, it does allow the PBL

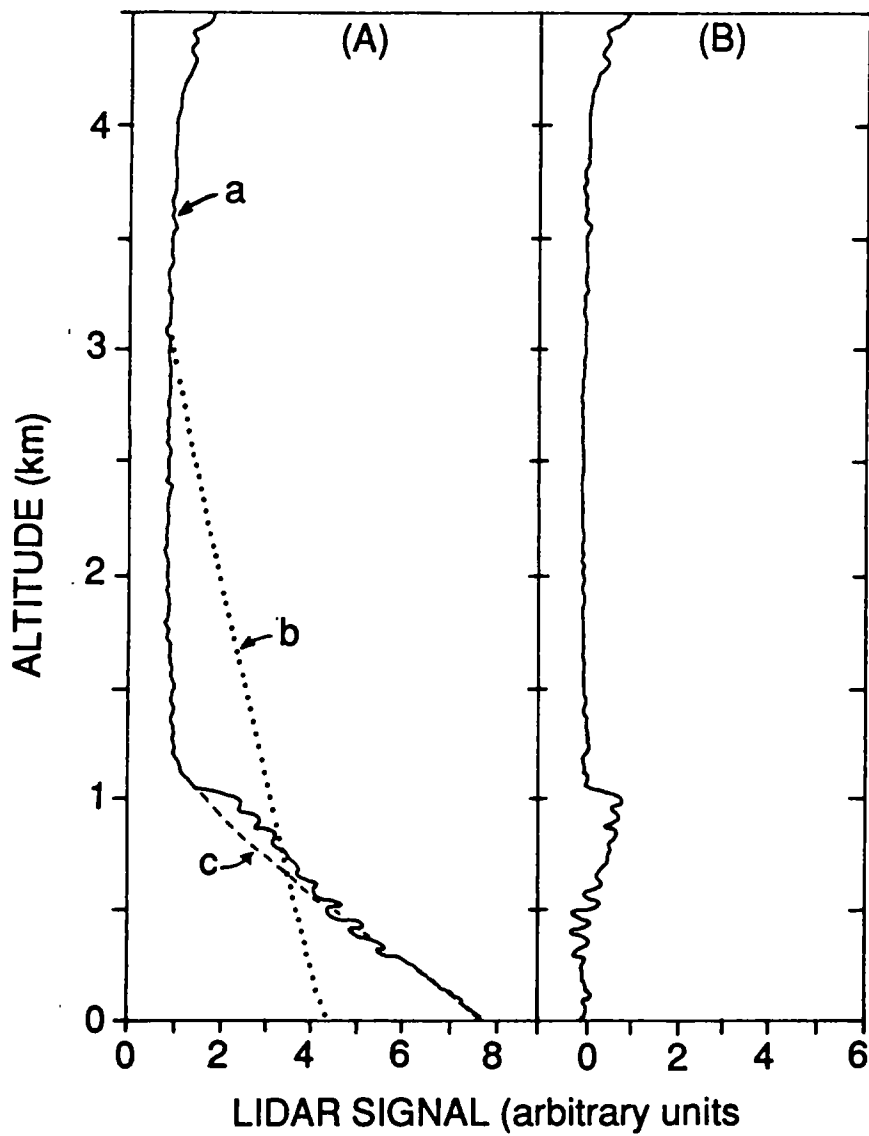


Figure 2. Lidar signal at  $1.064 \mu\text{m}$  measured at 1936 MST on 8 February 1989 at White Sands Missile Range, New Mexico. A) Line "a" is the uncorrected lidar signal, "b" the Rayleigh backscattering profile derived from the climatological sounding for February from El Paso, Texas, and "c" the polynomial fit used to correct the lidar signal near the surface. B) Signal corrected for amplifier problems.

signal to be observed in the following color cross-sections. The resulting signal after subtracting the polynomial is shown in figure 2B.

Figure 3 shows a two-dimensional, range-corrected, false-color, time-height, cross-section of the infrared signal. The data were taken from 1926 to 2016 MST on 8 February, 1989. The near-surface return has been modified in the manner described above. Oscillations caused by a transient signal are indicated by the letter "a". The signal we believe to be the top of the PBL is indicated by "b". At about 5 km above the surface (marked "c"), a layer of altocumulus (perlucidus) appears. This thin, water-droplet cloud allows transmission of a significant portion of the laser beam to higher altitudes. Although these clouds appeared to be at a single level when observed visually, the lidar cross-section shows that they possess considerable vertical structure. At 9-11 km, cirrus (fibratus) clouds appear (indicated by "d" in Fig. 3). Fallstreaks extend from the base of these clouds. No structure due to aerosol or cloud particles can be seen between 1.5 km and the altocumulus clouds.

Figure 4 shows a similar time cross-section taken from 2016 to 2100 MST on 8 February, 1989. Figure 5 shows data taken from 0820 to 1058 MST on 8 February. Note that the same cloud features are present: a low-level altocumulus layer, and a higher cirrus layer. This cloud pattern was present during almost all of the lidar operation periods. Figures 6-10 show additional cross-sections from data taken throughout the remainder of the project (see the figure captions for specific times).

Several attempts were made to extract quantitative values (backscatter and extinction coefficients) from the lidar profiles for both wavelengths. Because of the difficulties with the amplifier at the 1.064  $\mu\text{m}$  wavelength, we have focused our efforts on data from the visible wavelength signal (this wavelength corresponds most closely with aircraft nephelometric values and observations of meteorological range).

Figure 11 shows vertical profiles of extinction derived from lidar measurements at (a) 1936 MST on 8 February 1989, (b) 2057 MST on 8 February, and (c) 1159 MST on 9 February. The profiles of extinction were derived by assigning the Rayleigh backscattering value at 3.5 km to the lidar signal at this level, then subtracting the calculated Rayleigh profile (based on the climatological El Paso sounding) from the lidar return. Note that we have neglected the attenuation of the lidar beam by

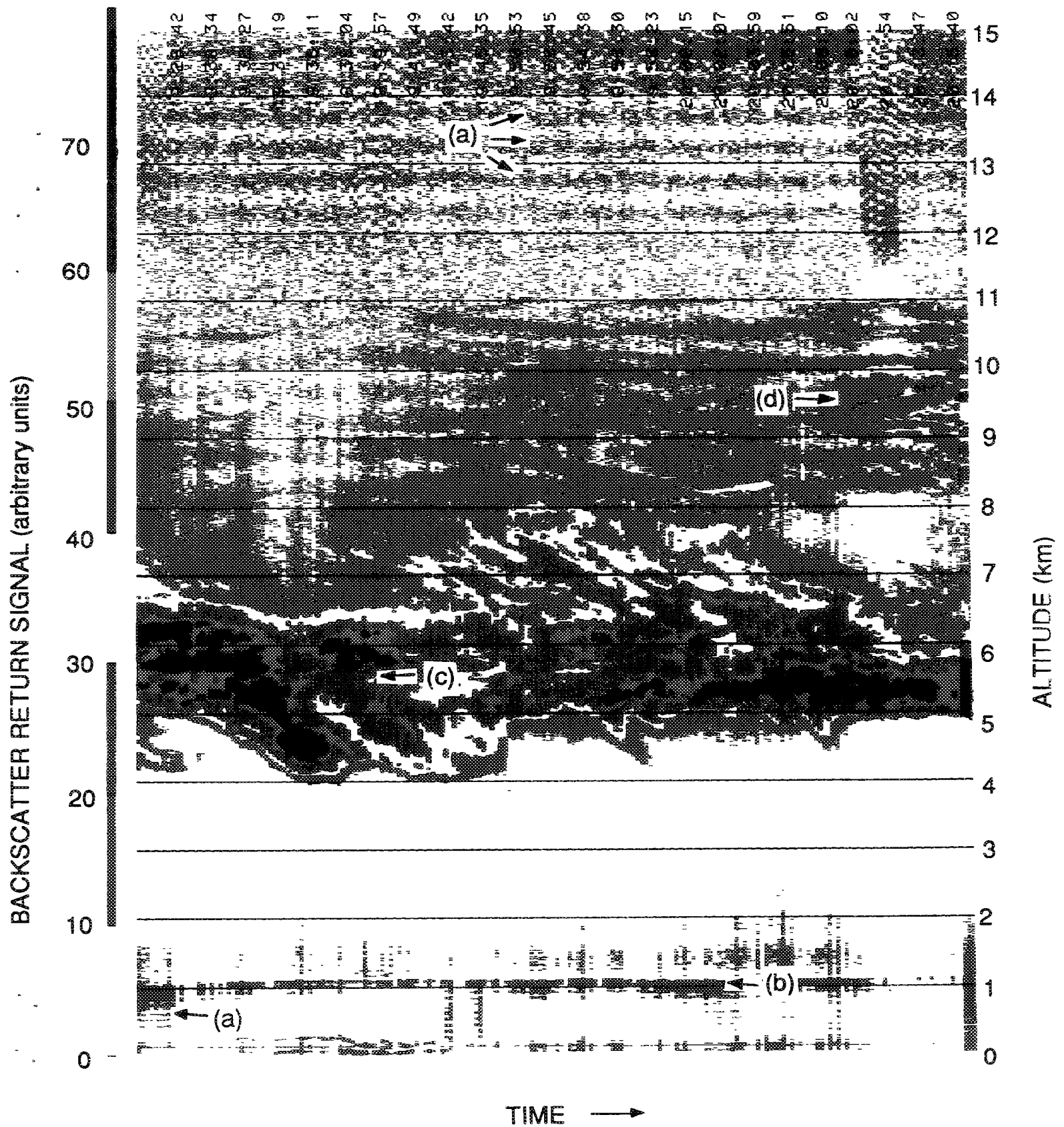


Figure 3. Time-height false-color cross-section of the lidar return signal at 1.064  $\mu\text{m}$  from 1926 to 2016 MST on 8 February 1989 after correction for near-surface errors. Features marked by "a" are spurious, induced electronic signals, "b" enhanced scattering at the top of the PBL, "c" a layer of altocumulus (perlucidus), and "d" a higher cirrus (fibratus) layer.

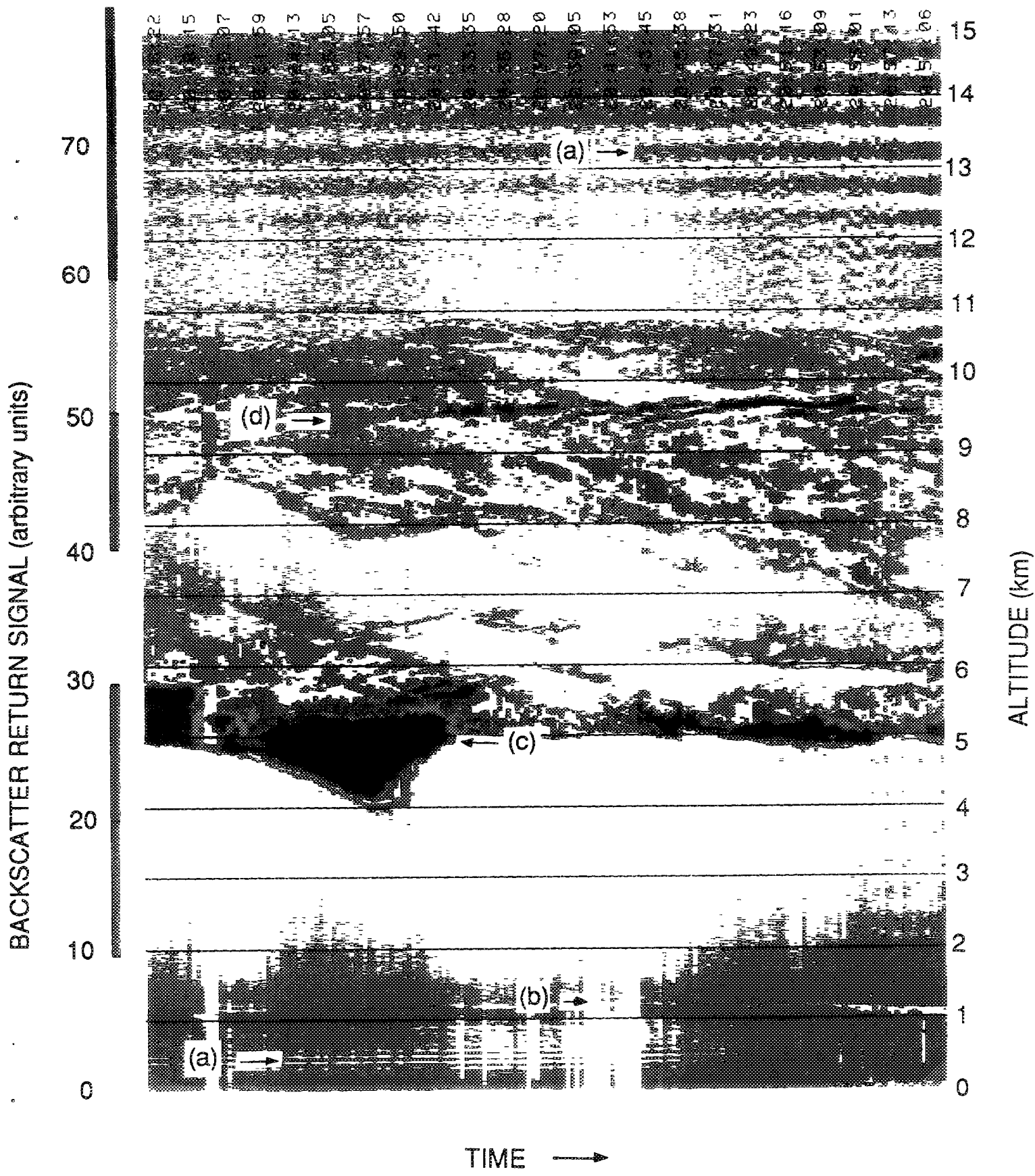


Figure 4. As for Figure 3, but from 2016 to 2100 MST on 8 February 1989.

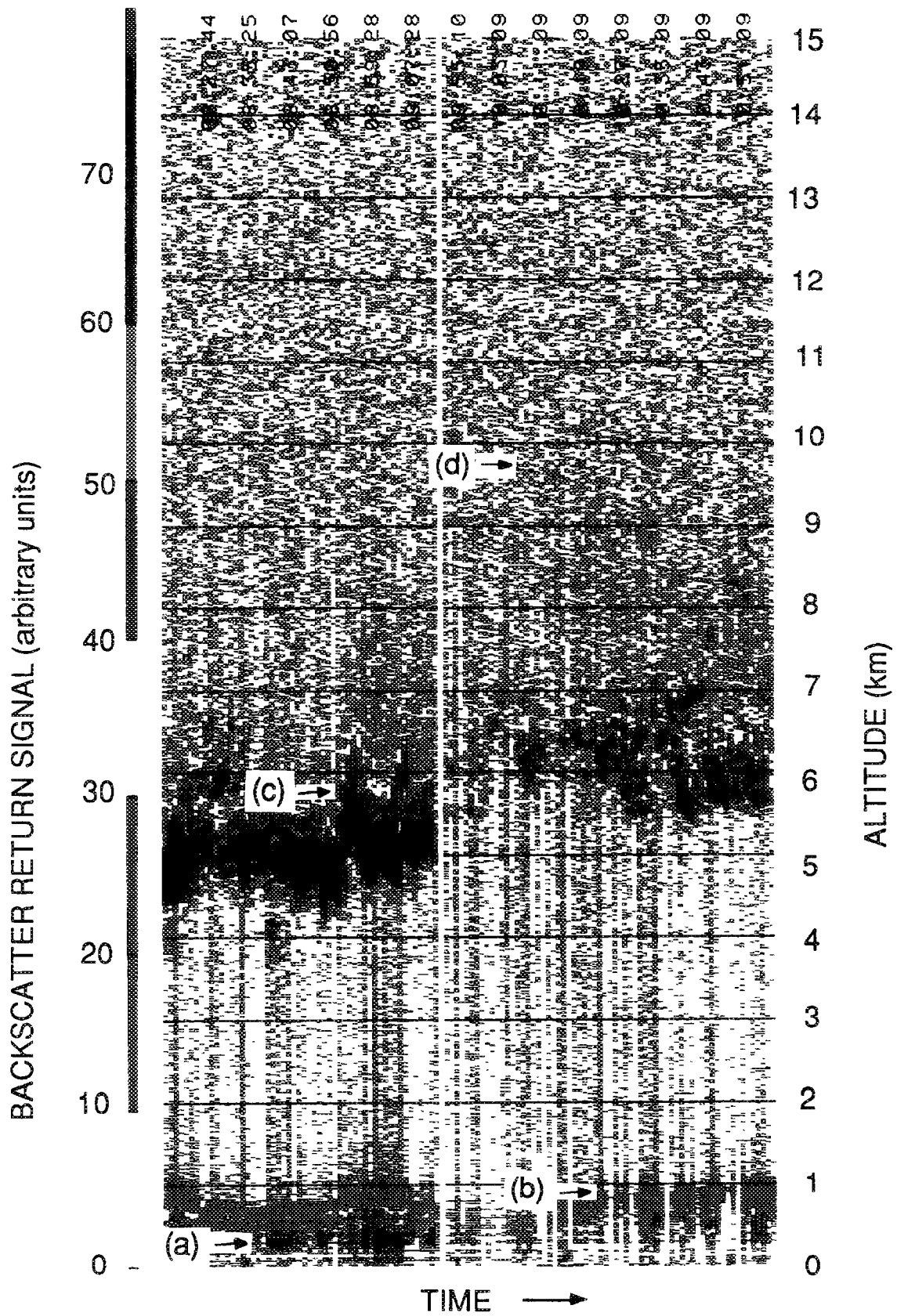


Figure 5. As for Figure 3, but from 0820 to 1058 MST on 8 February 1989.



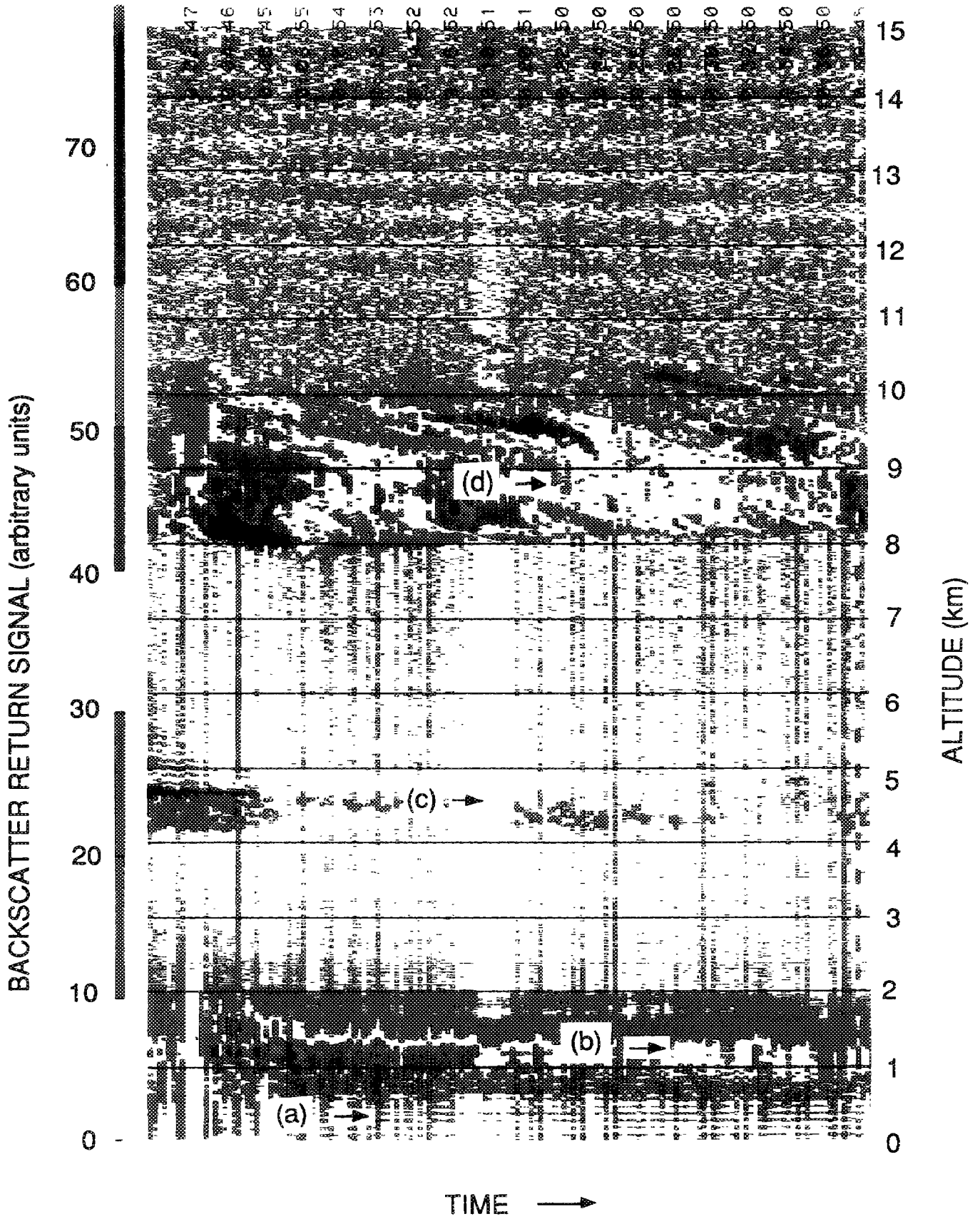


Figure 7. As for Figure 3, but from 1001 to 1039 MST on 9 February 1989.



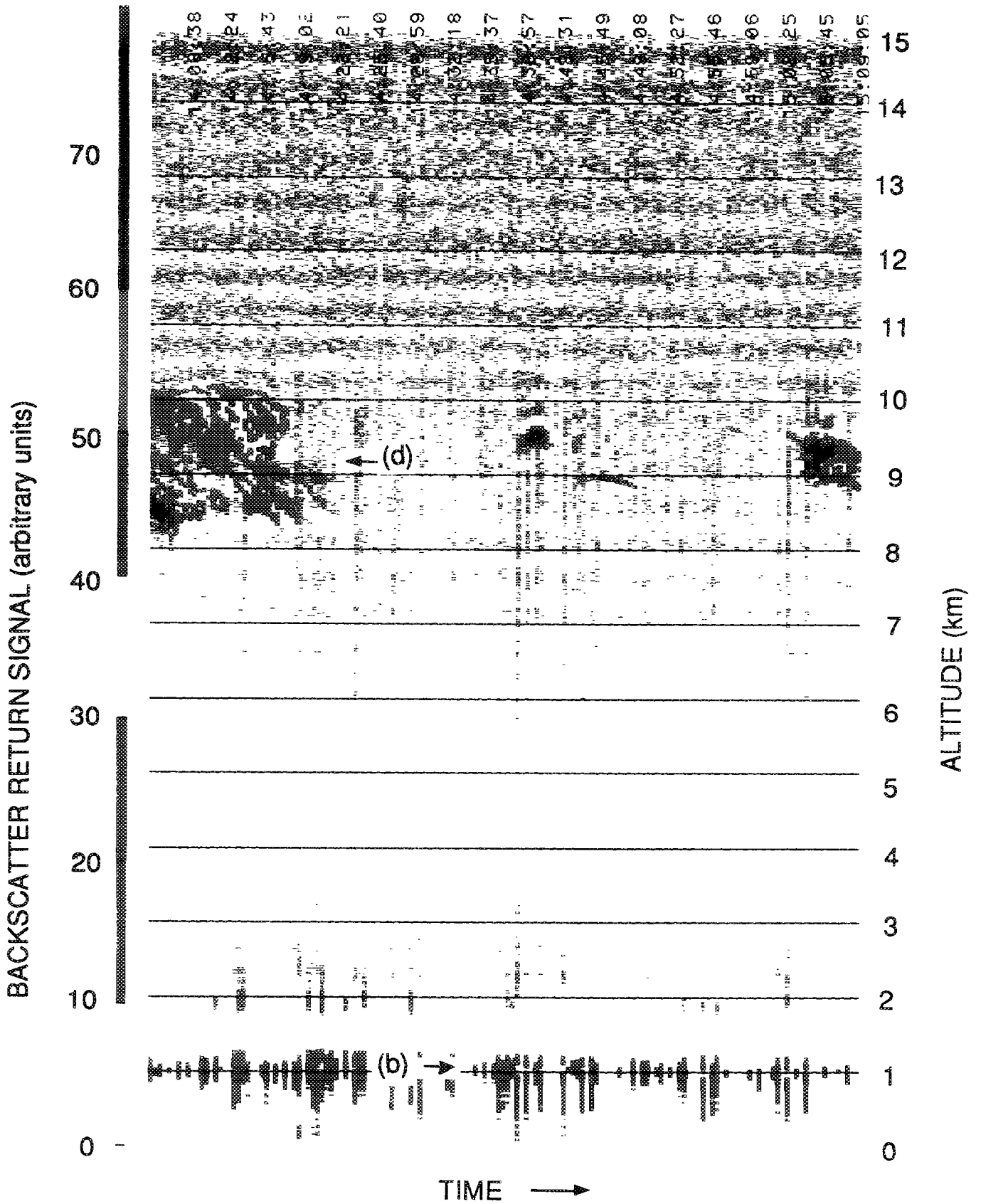


Figure 9. As for Figure 3, but from 1405 to 1509 MST on 9 February 1989.

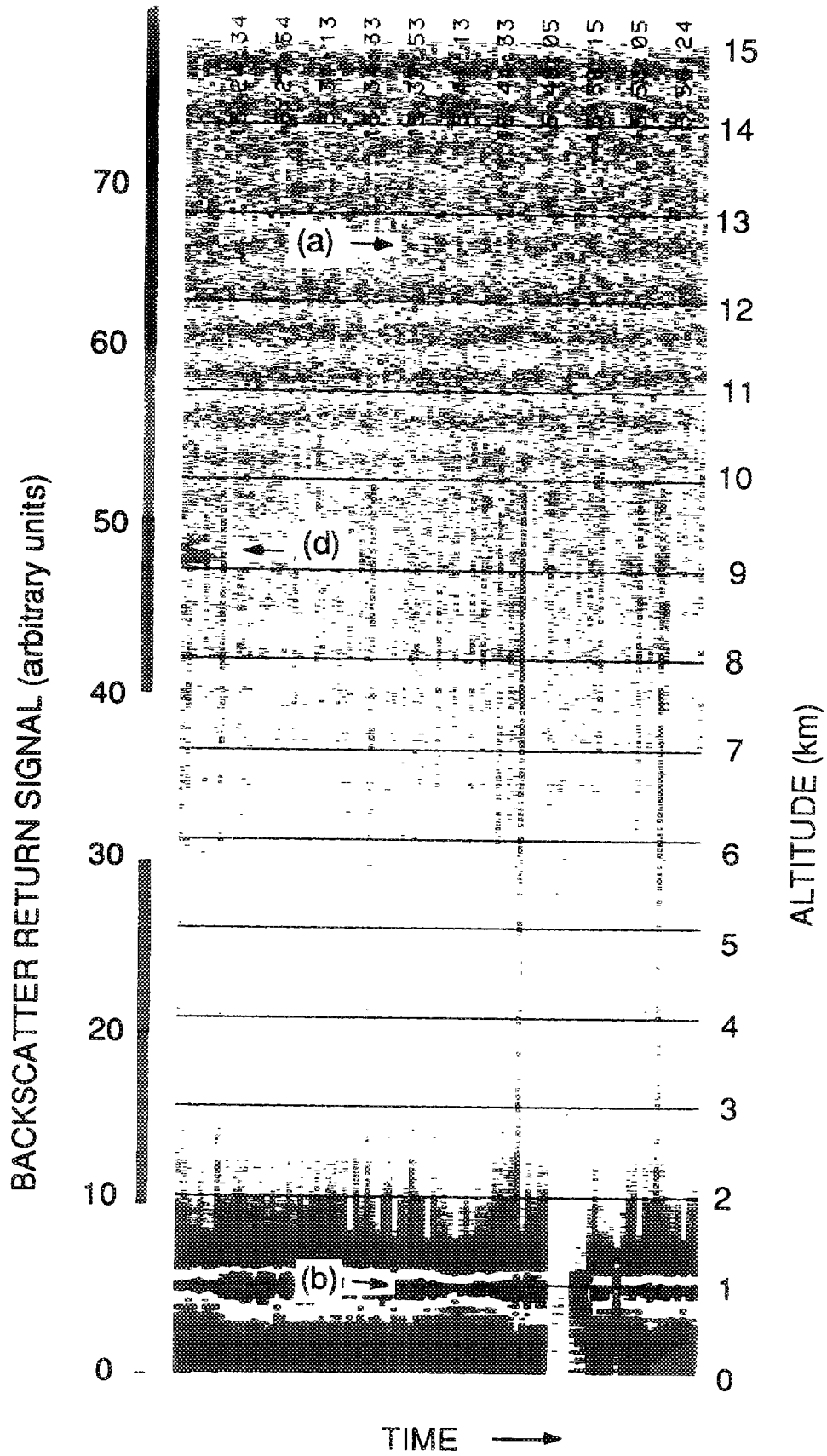


Figure 10. As for Figure 3, but from 1521 to 1559 MST on 9 February 1989.

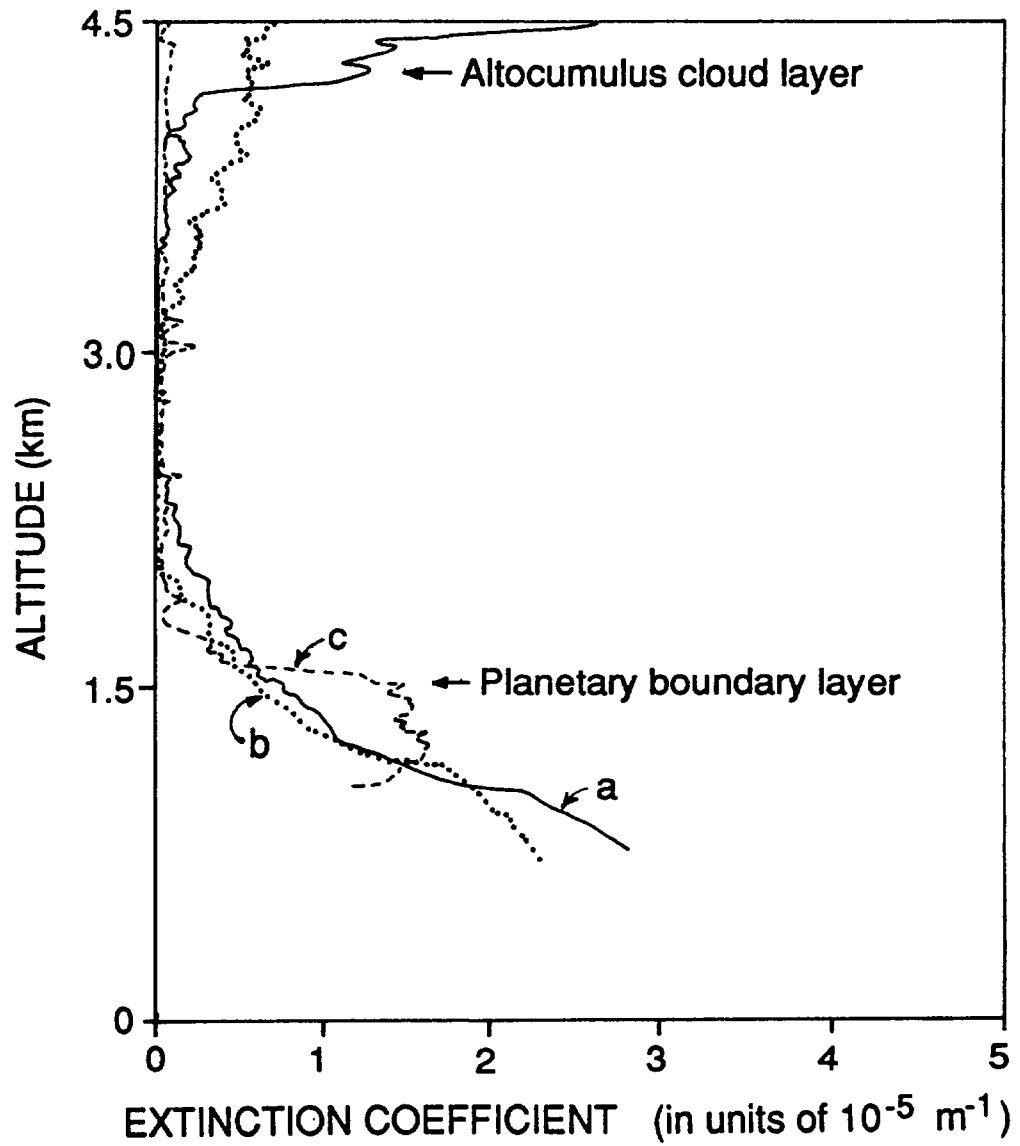


Figure 11. Vertical profiles of extinction at 0.532  $\mu\text{m}$  due to particles, as derived from lidar measurements at (a) 1936 MST on 8 February 1989; (b) 2057 MST on 8 February 1989; and (c) 1159 MST on 9 February 1989.

extinction (the exponential term in equation 1). This is a reasonable approximation for clear atmospheres (Klett, 1981). Visibilities in the lower troposphere were very high during the project at WSMR; we estimate that the meteorological range was in excess of 100 km when lidar data were taken. To derive values of optical extinction from the backscatter measurements, a measurement or a parameterization of the relation between the two variables is needed. Several authors have presented such parameterizations based on measurements (e.g. Fernald, 1971; Salemink *et al.*, 1984); We will use the value of  $\sigma_e/\beta=40$ , appropriate for a relative humidity of 60% (Salemink *et al.*, 1984). In general, Figure 11 shows that there was little optical structure between 1 km above the ground and cloud base; extinction coefficients were quite low. As discussed above, it was not possible to obtain quantitative information from the lidar signals below 1 km.

## 5. RECOMMENDATIONS FOR FUTURE WORK

Before this experiment is repeated, we recommend that a number of issues be addressed:

- a) The lidar system should be installed in an environmentally stable enclosure (e.g. a trailer) in order to reduce electrical failures.
- b) The lidar should be mounted in such a way that the beam can be directed at a number of angles from zenith to horizon. This will allow the lidar to fully explore the PBL structure in the quantitative region of the beam away from the near-field. It would also permit the calibration of the lidar using the slope method. As described by Salemink *et al.* (1984), the slope method can be used to relate backscatter to extinction in a homogeneous atmosphere. Equation 1 can be rearranged to yield (ignoring the contribution from multiple scattering):

$$P(r) r^2 = C \beta(r) \exp \left( -2 \int_0^r \sigma_e(r) dr \right), \quad (2)$$

where,  $\beta(r) = \beta_g(r) + \beta_p(r)$

Taking the logarithm of both sides of (2), and assuming that the extinction coefficient is unchanging across the region being examined, the lidar equation becomes:

$$\ln [P(r) r^2] = \ln [C\beta(r)] - 2\sigma_e r \quad (3)$$

Hence, by plotting measured values of  $\ln [P(r)r^2]$  against  $r$ , the slope and intercept can be determined, yielding values for  $\beta(r)$  and  $\sigma_e$ .

- c) In lieu of changing the orientation of the lidar beam to gain better information on PBL structure, the divergence of the laser might be increased from 1 mrad to a larger value through appropriate optical manipulation. This would have a negative impact on sensitivity at higher altitudes. An alternative would be to operate the lidar in a bistatic mode. Since the field of view of the telescope diverges more quickly with distance than does the laser beam, firing the laser next to the telescope (rather than at the focal point of the telescope assembly) at a slight angle inward toward the telescope would allow the beam to enter the telescope's field of view more rapidly. Both of these approaches are rather major modifications to the current lidar system.
- d) Clearly, the performance of the logarithmic amplifiers must be fully investigated; new amplifiers may need to be purchased. The poor condition of the electronic components and the telescope assembly upon arrival after shipping again points to the need for permanent installation in a mobile platform.

- e) To accurately solve the lidar equation in its full form, *in situ* aircraft observations of extinction made directly over the lidar site would be invaluable.

## 6. CONCLUSIONS

A joint research project between the University of Washington, the Georgia Tech Research Institute, and the National Oceanic and Atmospheric Administration was undertaken at White Sands Missile Range, New Mexico, to test a new lidar system and analyze initial data. The objectives of the lidar test were to examine the height and structure of the planetary boundary layer (PBL), to derive profiles of atmospheric extinction for comparison with nearby aircraft measurements, and to detect and examine the structure of visible and subvisible cirrus clouds. Of these three goals only the last one (observing cloud structure) was successfully met. Difficulties associated with the logarithmic amplifiers, induced electronic noise, and constant moving of the lidar system, made quantitative retrieval of extinction profiles impossible. These same problems, as well as difficulties caused by the slow divergence of the laser beam, made examination of PBL structure difficult, although the top of the PBL was detected. The lidar proved capable of detecting and mapping very thin cirrus clouds (including those formed by aircraft contrails) at altitudes up to 12 km, even through a layer of altocumulus cloud.

Before the lidar system is used for a similar study, installation problems (including those caused by induced noise) need to be rectified. This can best be accomplished by placing the lidar in a permanent mount on a mobile vehicle. The configuration should eventually allow for viewing at a variety of angles from zenith to horizon.

## REFERENCES

- Collis, R. T. H. and P. B. Russell. Lidar measurement of particles and gases by elastic backscattering and differential absorption. In Laser Monitoring of the Atmosphere, E. D. Hinckley, Ed. 71-151, Springer-Verlag, Berlin, 1976.
- Eloranta, E. W. and D. K. Forest. Generation of attenuation corrected images from lidar data. Proc. 13th Int'l Lidar Conf., NASA Conf. Publ. 2431, 334, 1986.

- Fernald, F. G., Herman, B. M. and J. A. Reagan. Determination of aerosol height distributions by lidar. J. Appl. Meteor., 11, 482-489, 1971.
- Klett, J. D. Stable analytic inversion solution for processing lidar returns. Appl. Optics, 20, 211-220, 1981.
- Koschmieder, H. Theorie der horizontalen Sichtweite. Beitr. Phys. Freien Atm. 12, 33-53: 171-181, 1924.
- Kunz, G. J. Vertical atmospheric profiles measured with lidar. Appl. Optics, 13, 1953-1957, 1983.
- Martin, C. L., Fitzjarrald, D. Garstang, M., Oliveira, A. P., Greco, S. and E. Browell. Structure and growth of the mixing layer over the Amazonian rain forest. J. Geophys. Res., 93, 1361-1375, 1988.
- McElroy, J. L., Eckert, J. A. and C. J. Hager. Airborne downlooking lidar measurements during STATE 78. Atmos. Environ., 15, 2223-2230, 1981.
- Melfi, S. H., Spinhirne, J. D. and S.-H. Chou. Lidar observations of vertically organized convection in the planetary boundary layer over the ocean. J. Clim. Appl. Meteor., 24, 806-821, 1985.
- Platt, C. M. R. Lidar and radiometric observations of cirrus clouds. J. Atmos. Sci., 30, 1191-1204, 1973.
- Platt, C. M. R. Remote sensing of high clouds: I. Calculation of visible and infrared properties from lidar and radiometer measurements. J. Appl. Meteor., 18, 1130-1143, 1979.
- Reed, R. K. Comparison of measured and estimated insolation over the eastern Pacific Ocean. J. Appl. Meteor., 21, 339-341, 1982.
- Salawitch, R. J., Wofsy, S. C. and M. B. McElroy. Influence of polar stratospheric clouds on the depletion of Antarctic ozone. Geophys. Res. Letts., 15, 871-874, 1988.
- Salemink, H. W. M., Schotanus, P. and J. B. Bergwerff. Quantitative lidar at 532 nm for vertical extinction profiles and the effect of relative humidity. Appl. Phys., B-34, 187-189, 1984.
- Sassen, K., M. K. Griffin. and G. C. Dodd. Optical scattering and microphysical properties of subvisual cirrus clouds, and climatic implications. J. Appl. Meteor., 28, 91-98, 1989.
- Shiple, S. T., Tracy, D. H., Eloranta, E. W., Trauger, J. T., Sroga, J. T., Roesler, F. L. and J. A. Weinman. High spectral resolution lidar to measure optical scattering properties of atmospheric aerosols. 1: Theory and instrumentation. Appl. Optics, 22, 3716-3724, 1983.
- SMIC, Study of Man's Impact on Climate. MIT Press, Boston, 1971.
- Spinhirne, J. D., Reagan, J. A. and B. M. Herman. Vertical distribution of aerosol extinction cross-section and inference of aerosol imaginary index in the troposphere by lidar technique. J. Appl. Meteor., 19, 426-438, 1980.
- Sroga, J. T., Eloranta, E. W., Shipley, S. T., Roesler, F. L. and P. J. Tryon. High spectral resolution lidar to measure optical scattering properties of atmospheric aerosols. 2: Calibration and data analysis. Appl. Optics, 22, 3725-3732, 1983.

van de Ven, M. J. M., Noorman, C. J. and C. W. Lamberts. Coastal aerosol measurements. J. Aerosol Sci., 11, 281-292, 1980.

Waggoner, A. P. and L. F. Radke. Enhanced cold cloud clearing by pulsed CO<sub>2</sub> lasers. (Accepted for publication in Appl. Optics), 1989.

Warren, S. G., Hahn, C. J., London, J., Chervin, R. M. and R. L. Jenne. Global distribution of total cloud cover and cloud type amounts over land. DOE/ER/60085-H1 or NCAR/TN-273+STR, 1986.

Wendling, P., Wendling, R., Renger, W., Covert, D. S., Heintzenberg, J. and P. Moerl. Calculated radiative effects of arctic haze during a pollution episode based on ground-based and airborne measurements. Atmos. Environ., 19, 2181-2193, 1985.

Wylie, D. P. and W. P. Menzel. Two years of cloud cover statistics using VAS. J. Climate, (In press), 1989.